A New Low-Cost Centralized MPPT Controller System for Multiply Distributed Photovoltaic Power Conditioning Modules

Sol Moon, Sung-Guk Yoon, *Member, IEEE*, and Joung-Hu Park, *Senior Member, IEEE*

***Abstract*—In this paper, an integrated maximum power point tracking (MPPT) controller system using a ZigBee wireless communication module is proposed for multimodal power converters as a concept of an intelligent photovoltaic (PV) module of PV power conditioning systems. The proposed scheme can integrate all information under a single host controller to realize low-cost manufacturing. It can also simplify the monitoring and supervision processes through machine-to-machine communications for the smart-grid. The voltage and current information for each module are periodically sampled and transferred to the central inverter (or another host server) through the ZigBee module. After the transmission process, the MPPT control algorithm derives each of the PV voltage reference parameters to return to each PV module accordingly. The technical benefits of the proposed approach is the configuration of a PV-controller system composed of a single digital-signal processor (DSP), low-cost analog controllers, and some mandatory communication peripherals used to monitor the distributed multimodules. Also, the method is quite desirable for supervision and monitoring of the overall system due to its centralized control structure. For the experimental validation of the proposed MPPT control, multiple ZigBee (XBee-PRO series) modules, as well as a DSP, dual-module solar simulators, and a couple of 50 W dc–dc power conversion hardware prototypes were utilized.**

***Index Terms*—Communication networks, machine-to-machine, maximum power point tracking (MPPT), photovoltaic (PV) systems, ZigBee.**

I. Introduction

STAND-ALONE or grid-tied photovoltaic (PV) systems have been used traditionally in buildings. These systems require an extra installation area, which presents an additional cost factor. However, the rooftop PV power system or the building-integrated PV (BIPV) system recently emerged as a solution to the problem of an extra installation area. The rooftop PV power system is a system that employs one or more PV panels installed on rooftops of residential or commercial buildings, whereas the BIPV system integrates the PV structure with an exterior building component like a roof or façade. Hence, it requires no additional installation and maintenance space. Conventional separate-installation techniques suffer from serious transmission losses when the generated power is transmitted to loads over long distribution networks. On the other hand, rooftop and BIPV systems allow for short-distance power transmission between the panels and the load inside the building, significantly reducing transmission loss [1]–[4]. Therefore, the rooftop and BIPV concept is considered the most suitable for distributed power systems in a smart grid as well as in localized power plants in urban areas.

To achieve a sufficiently high-voltage range using PV modules, multiple PV modules are connected in series. There are several kinds of architectures for multiple PV modules to interface with a grid. The simplest structure is shown in Fig. 1(a). It is a conventional type of central inverter with multiple PV modules [5]–[10]. This type of inverter is preferred due to its high-power capacity and low-manufacturing cost for a single power conditioning system (PCS). However, some low-efficiency operations occur in partial shading conditions due to the centralized maximum power point tracking (MPPT) controller as well as from losses in the string diodes.

Fig. 1(b) shows another type of PV system, the so-called multistring system, composed of a pair of dc/dc converters and a cascaded inverter for each PV string [11]. This type shows better performance than the centralized system in terms of maintenance, power losses upon failure, efficiency, and capacity expansion. However, it requires the string-level MPPT controller, which degrades power generation efficiency under partial shading in certain modules.

Finally, Fig. 1(c) shows the architecture for module integrated converters (MICs) with a centralized inverter for individual MPPT control based on the concept of the distributed MPPT (DMPPT) method [11]–[14]. Because of the individual MPPT controller in each PV panel, the control architecture maintains high-MPPT efficiency even under partial shading conditions in the PV structures. Therefore, it is considered the most ideal type of converter architecture for distributed power sources such as rooftop and BIPV modules. However, the high performance of the MIC-scheme is obtained at the cost of installing distributed MPPT controllers

Manuscript received January 9, 2014; revised May 28, 2014, September 10, 2014, January 7, 2015, and April 3, 2015; accepted May 23, 2015. This work was supported by the Human Resources Development of Korea Institute of Energy Technology Evaluation and Planning (KETEP) grant funded by the Korea government Ministry of Trade, Industry, and Energy (No. 20134010200570). Paper no. TSG-00020-2014. *(Corresponding author: Joung-Hu Park.)*

The authors are with the Department of Electrical Engineering, Soongsil University, Seoul 156-743, Korea (e-mail: nigabest@naver.com; sgyoon@ssu.ac.kr; wait4u@ssu.ac.kr).

Color versions of one or more of the figures in this paper are available online at http://ieeexplore.ieee.org.

Digital Object Identifier 10.1109/TSG.2015.2439037

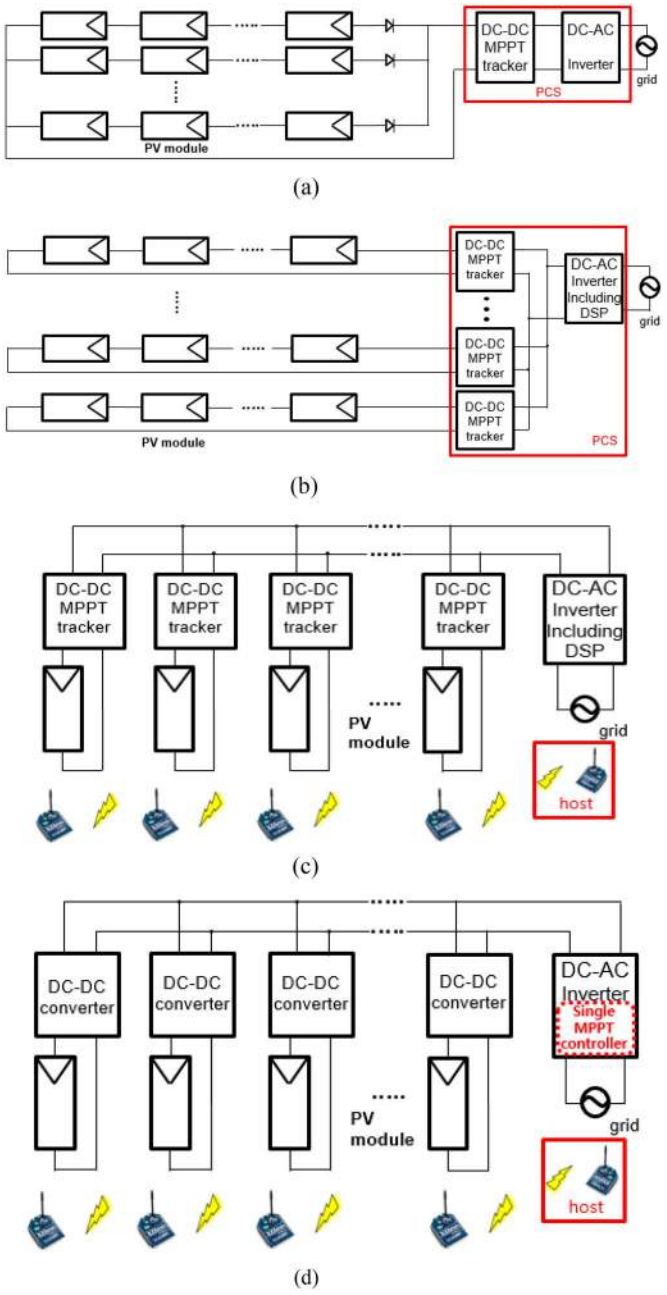

Fig. 1. Various types of PV PCSs. (a) Centralized PCS. (b) Multistring PCS. (c) MIC with a central inverter. The ZigBee is used for remote protection and supervisory control. (d) Proposed MPPT method along with ZigBee module. The ZigBee is used for MPPT as well as monitoring (PV protection, anti-theft, energy management, and so on).

and communication systems such as ZigBee[1] for each PV module as shown in Fig. 1(c). Therefore, the manufacturing cost of this scheme proportionally increases with the number of PV modules, which presents a huge barrier to the popularization of distributed PV power systems. To reduce the manufacturing cost for the MIC scheme, research on sensing, MPPT, control circuit, and communication parts must be efficiently coordinated [15]–[17]. The need to adopt both central MPPT (CMPPT) and DMPPT was investigated in [18]–[20].

In this paper, a new control architecture for PV power systems is proposed to reduce the manufacturing cost for PV systems while maintaining the same level of efficiency for the MIC scheme. It consists of a host MPPT controller in the centralized grid-tied inverter and a number of remote PV-MICs as shown in Fig. 1(d). The remote converter installed in a PV module is composed of an analog-circuited simple controller and a ZigBee module to enable control of the PV module by the host controller. The single MPPT controller contributes to the intelligent but low-cost PCSs in simpler, small/medium scale PV power sources. From the principle, the scheme can be called "integrated" MPPT control. Note that, the communication networks in Fig. 1(c) and (d) cost the same since both use the ZigBee wireless communication system and the same number of ZigBee devices.

Through ZigBee, the CMPPT controller obtains the current and voltage levels of each PV module. Using the data, the controller selects the reference voltage, which is necessary for each PV module to properly control the converter output. The reference voltage is sent back to each PV module through ZigBee. Therefore, with the exception of the ZigBee module, the PV module is composed of analog devices, which is the key to cost reduction.

Actually, a conventional state-of-the-art engineering of the concept was presented in [21] and [22]. The main portion of the centralized MPPT controller for PV modules was partially unified; however, it shared peripheral functions with the local controllers using digital-signal processors (DSPs) due to the absence of communication. The key issue in the conventional paper was the reduction of cost by eliminating the current sensor, rather than by complete MPPT controller unification.

This paper is organized as follows. First, the operating principle and design procedure of the proposed control scheme are presented in Section II. Section III presents the communication method between the PV controller and DSP (host controller) under the application programming interface frame. Simulation results are given in Section IV. Section V presents the experimental verification, and Section VI discusses cost reduction and practical issues. Finally, the conclusion is presented in Section VII.

II. Operating Principle and Design Consideration

A. Operating Principle

Fig. 2 shows the centralized MPPT controller with the peripheral communication setup for the proposed scheme. A digital-processor-based host controller in the post power-integration stage, the dc/ac inverter in this case, contains an integrated MPPT controller that replaces the individual controllers for finding the respective maximum power points of the remote multiple power-conditioning modules. For the sake of centralization, all the module information for the perturbation and observation (P&O) algorithm, such as PV voltage and current, is sent to the host with other peripheral data. After the

[1]In this paper, we use the ZigBee module as a communication system. However, according to the number of PV modules and the distance between PV panels, any communication system, such as Bluetooth or Wi-Fi, can be installed. Choosing the most appropriate communication system for the PV system is beyond the scope of this paper.

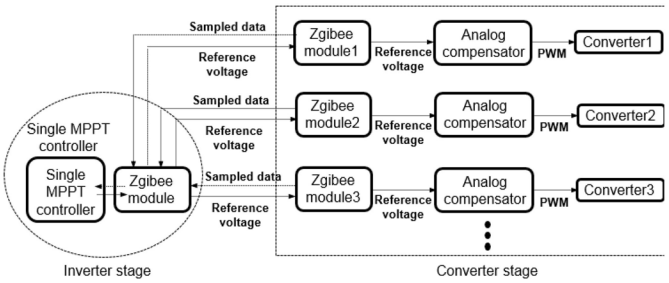

Fig. 2. Block diagram of integrated MPPT controller and the peripheral communication structures for the realization of proposed method.

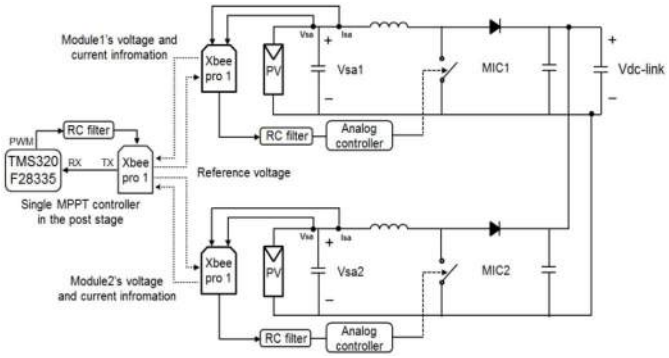

Fig. 3. Proposed MPPT scheme with parallel-connected boost type MICs.

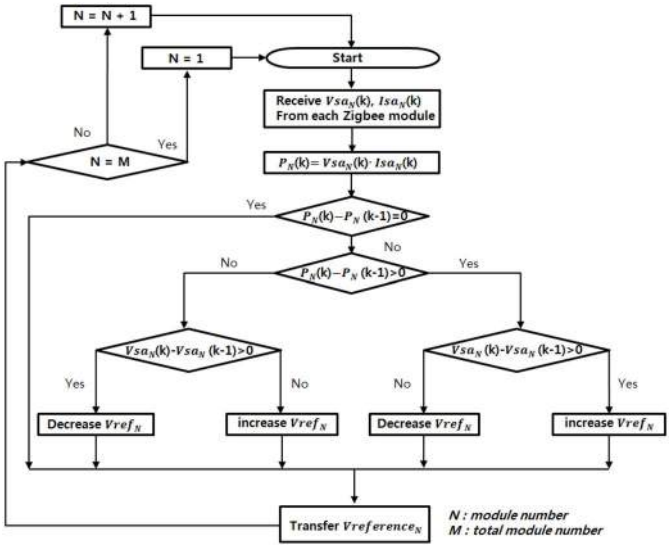

Fig. 4. Centralized MPPT algorithm of multiple local PV modules.

algorithm updates the PV reference, the updated reference is transmitted back to the individual converters through the same route. Therefore, the required function of the local controller in the PV module converter is nothing but a single loop control, easily realizable even with analog circuitry and the peripheral interfaces. By integrating the controller, system-level cost can be reduced. The detailed cost reduction is presented in Section VI-A.

To this end, proper communication networks are necessary. This type of configuration can be categorized as machine-to-machine communications, which enables communication components embedded in a smart device to reply to external requests or to transmit data for interconnection, networking, and remote controllability with low cost, high scalability, and good reliability.

In this paper, the ZigBee, i.e., XBee-PRO, is used to connect each PV module to the central controller. Fig. 3 shows a more detailed description of the proposed MPPT control system with step-up converters based on an analog controller and ZigBee devices. The simple analog controllers contribute significantly to cost reduction compared to the conventional digital controllers shown in Fig. 1(c). The XBee-PRO is composed of an RF module with peripheral processors, and provides basic functions such as an analog-to-digital converter (ADC), pulse-width modulation (PWM), and hibernation mode for low-power consumption.

Fig. 3 also shows the signal flow between the local MICs and host DSP (central). Each individual PV panel's voltage and current information are converted to UART data format and transmitted to the host via the ZigBee module in every sampling period. Then, the host controller at the central DSP rapidly executes the P&O algorithm for efficient MPP tracking of each module. The perturbed PV reference out of the DSP is transmitted back to the local converter through the same path at every P&O cycle. The following section presents a more detailed description of the MPPT operating principle.

B. Maximum Power Point Algorithm

Fig. 4 shows the MPPT algorithm used for the proposed control method. The main body of the algorithm is the same as that of the conventional P&O method. However, when the algorithm is applied to multiple module systems, the sequence for the MPPT reference update should be taken into consideration. For example, one previous report has suggested an MPPT sequence in which the next module's reference begins tracking the MPP after the previous other module has completed its tracking routine [21], [22]. Therefore, if the PV-voltage settling time at a step of the reference update takes Ts, then the next module should wait for the number of MPP-tracking steps in multiple times of Ts, which makes the tracking speed very slow. On the other hand, the proposed controller distributes the updated references to each module in turn, without waiting for the settling time. For example, a module can update the PV reference during the settling response of the previous other module since the modules do not need to wait for the previous module's MPP arrival. Therefore, this method can provide high-MPP tracking speeds, unlike the previous multimodal MPPT method. Consequently, the MPPT efficiency of the proposed is almost the same as that of the individual MPPT controller. This is because the PV transient response is quite slow compared to the DSP and communication speed. The detailed sequence of the algorithm is shown in Fig. 4. The MPP performances are shown in Fig. 18 of the experimental results section.

C. Compensator Design

After a local controller receives the updated PV reference, the PV module converter begins to regulate the PV voltage

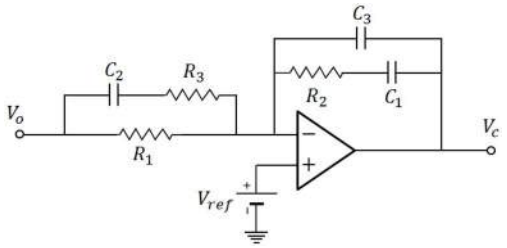

Fig. 5. Three-pole two-zero compensator.

TABLE I
TRANSFER FUNCTION AND CORRESPONDING FREQUENCIES OF PID COMPENSATOR

Transfer function ($\omega = 2\pi f$)	$G_c(s) = \frac{w_I}{s} \cdot \frac{(1+{}^{s}/_{\omega_{z1}})(1+{}^{s}/_{\omega_{z2}})}{(1+{}^{s}/_{\omega_{p1}})(1+{}^{s}/_{\omega_{p2}})}$
ω_I	${}^{1}/_{R_1C_1}$
ω_{Z1}	${}^{1}/_{R_2C_2}$
ω_{Z2}	${}^{1}/_{R_1C_2}$
ω_{P1}	${}^{1}/_{R_3C_2}$
ω_{P2}	${}^{1}/_{R_2C_3}$

TABLE II
RESISTANCES AND CAPACITIES OF THE COMPENSATOR

Parameter	Value
R_1	910Ω
R_2	$885.7821 \approx 910\Omega$
R_3	$15.5813 \approx 16\Omega$
C_1	$4.3724 \cdot 10^{-7} \approx 0.47$uF
C_2	$8.5121 \cdot 10^{-7} \approx 0.82$uF
C_3	$8.9839 \cdot 10^{-9} \approx 8200$pF

in accordance with the reference by adjusting the PWM duty cycle of the boost switch. In addition to the reference, the PV-sensing voltage is needed to construct a feedback control for the PV voltage. Stable operation requires a sufficient phase margin, typically greater than 45°. To guarantee the phase margin, a compensator is inserted between the sensor and PWM generator. There are several kinds of compensator circuits according to the number of poles and zeros: PI, PD, and PID. In this paper, a PID compensator with three-pole and two-zero is used. The compensator can be easily implemented with purely analog devices as shown in Fig. 5. Table I presents the transfer function and corresponding frequencies of the PID compensator. The values of the resistances and capacitors are listed in Table II.

For the closed-loop design, the frequency response of the converter's transfer function, such as control-to-output, $G_{\mathrm{vd}}(s)$, is necessary. The transfer function is derived by a state-space averaging technique under the small-signal assumption. The transfer functions are derived, as shown in Table III, and Bode plots of the frequency responses are shown in Fig. 6. The product of the sensor and PWM generator gain is unity. From the results, the poles and zeros of the compensator $G_c(s)$ are fixed for the final loop-gain $T(s)$. The design result shows a 57° phase margin along with the 2.2 kHz cut-off frequency.

TABLE III
FINAL TRANSFER FUNCTION, COMPENSATOR, AND THE LOOP GAIN

$G_{vd}(s)$	$\frac{-120}{6 \cdot 10^{-7}s^2 + 2.344 \cdot 10^{-5}s^2 + 1}$
$G_c(s)$	$\frac{-0.000754s^2 - 2.92s - 2513}{1.055 \cdot 10^{-10}s^3 + 2.122 \cdot 10^{-5}s^2 + s}$
$T(s)$	$\frac{0.008324s^2 + 32.24s + 2.775 \cdot 10^4}{6.333 \cdot 10^{-17}s^5 + 1.273 \cdot 10^{-11}s^4 + 6.006 \cdot 10^{-7}s^3 + 4.466 \cdot 10^{-5}s^2 + s}$

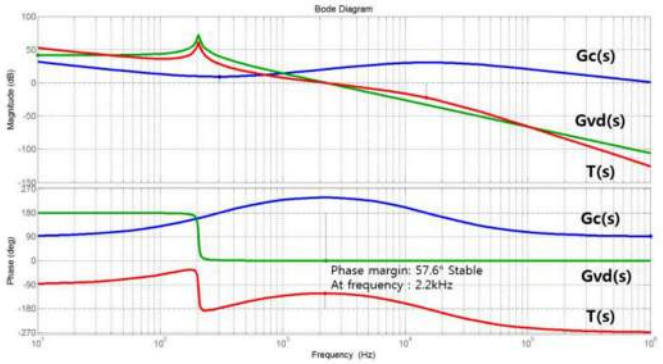

(a)

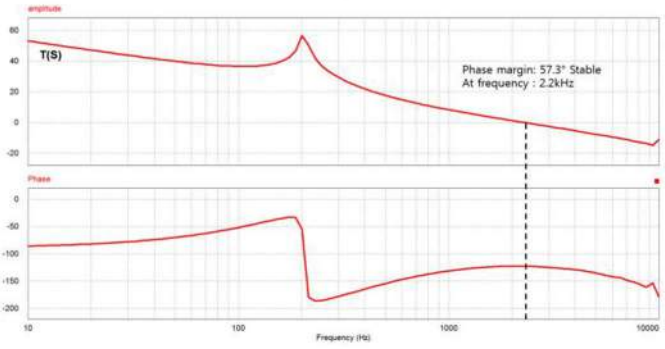

(b)

Fig. 6. Compensator design and closed-loop response (a) bode plots of the derived transfer functions and the loop gain in MATLAB and (b) numerical analysis of the exact-switching model with PSIM software.

Fig. 6 shows not only the Bode plots of the loop gain for the converter's averaged model, but also the frequency response obtained from computer simulations using the frequency-sweep of an exact nonlinear (switching) time-domain model built by the PSIM tool. Comparing the Bode plots, it can be seen that both loop gains agree well with each other, verifying the averaged-analytical model (the loop gain).

III. COMMUNICATION MODULE

ZigBee has been spotlighted as a leading technology for wireless sensor networks due to its low power and cost. Originally, ZigBee was designed to overcome the limitations of Wi-Fi and Bluetooth [23]. Wi-Fi provides higher data rate, but it consumes much more power than both ZigBee and Bluetooth. The data rate for Bluetooth is higher than that of ZigBee but both technologies have similar power consumption.

TABLE IV
SPECIFICATION OF THE XBee-PRO SERIES1 [25]

Indoor/Urban Range	Up to 300ft. (100m)
Outdoor RF line-of-sight Range	Up to 1mile (1500m)
Transmit Power Output	63mW
RF data Rate	250,000bps
Serial interface Data Rate	1200bps-250kbps
Receiver Sensitivity	-100dBm

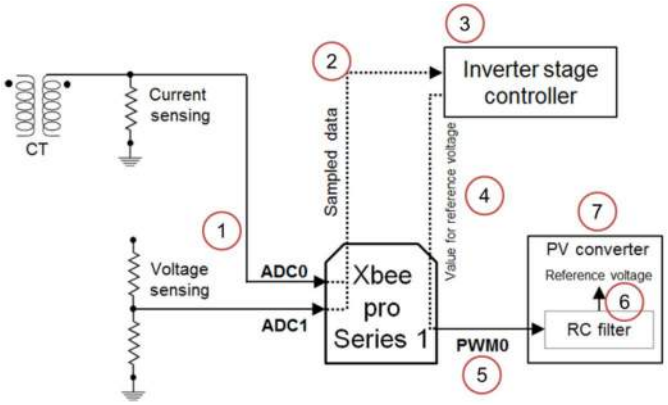

Fig. 7. Overall flow for the low-cost centralized MPPT controller system.

However, a Bluetooth network supports only star topology and seven devices. Although ZigBee provides the lowest data rate, it supports various topologies and many devices in a network with low-power consumption. Because of these features, ZigBee is a viable technology for smart grid home area networks [24].

In this paper, we use the XBee-PRO series1 to connect the central controller to the remote PV modules. Table IV shows detailed specification for the XBee-PRO series1. We chose the XBee-PRO series1 (MC13191 RF device with MC9S08GT60 controller) because it provides an input/output line passing function. The input/output line passing function creates a virtual wire between XBee modules [25].

Fig. 7 shows the overall flow for our proposed system. First, current and voltage information for a PV module is sensed (no. 1). Then, the information is sent to the central host in digital format through XBee-PRO (no. 2). With the data, the central host selects a reference voltage using the MPPT algorithm in Section II-A (no. 3). The reference voltage is delivered to the PV module through XBee-PRO (no. 4). XBee-PRO outputs the reference voltage in PWM format (no. 5). By passing through an RC filter, the PWM data is converted to analog data (no. 6). Finally, the PV converter uses the analog reference voltage (no. 7).

A. Transmission From PV to the Host Controller

To transfer the current and voltage information for a PV module, two data-input channels, i.e., ADC0 and ADC1, are needed. As shown in Fig. 7, the current and voltage analog data are converted to digital data through an ADC with a 10-bit ADC resolution provided by XBee-PRO. The data is transferred to the central host using the input/output line passing function. With this function, the sampled data is periodically transferred to the XBee-PRO at the central host under an arbitrary time interval by simply setting a sample rate in Fig. 8. The desired ZigBee channels can be activated with this software. Detailed parameters, i.e., sample rate and status monitor, can be adjusted with the input/output line passing command, as shown in Fig. 8. The ZigBee then transfers the information to the DSP through the standard serial communication interface.

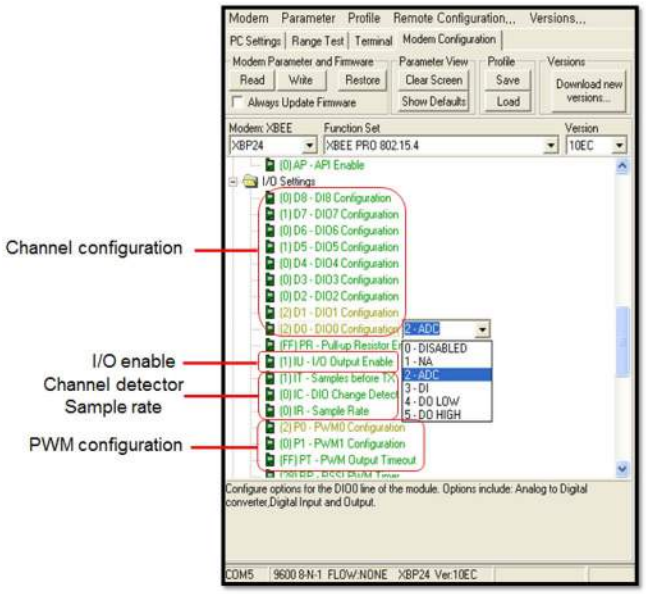

Fig. 8. Screen capture of the I/O setting part in XCTU-software for channel activation of ZigBee device.

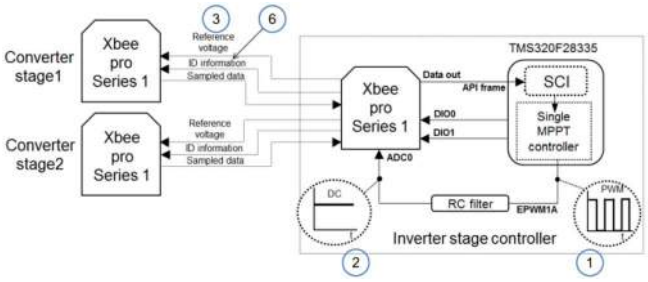

Fig. 9. Information flow from the host controller to multiple PV converters.

B. Transmission From the Host Controller to the PV

Unlike the central host, the PV converter in the PV module needs the reference PV voltage in analog form. However, analog output is not provided by XBee-PRO. To provide analog data to the PV converter, two operations are proposed: analog reference voltage transfer operation to the PV converter and PV-module identification operation among multiple PV modules.

1) Analog Reference Voltage Transfer Operation: To create an analog value at the host, a PWM output from the DSP (no. 1) and RC filter are used as shown in Fig. 9. ADC0 of XBee-PRO in the host receives the analog data (no. 2). Using the pin pairing method, which is provided by

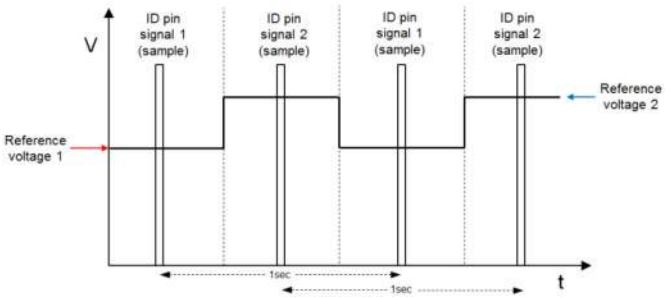

Fig. 10. Operation example for the reference voltage distribution and ID information scheme. The bit (pulse) signal at a specific digital output pin is the ID information and the rectangular signal is the instantaneous reference voltage.

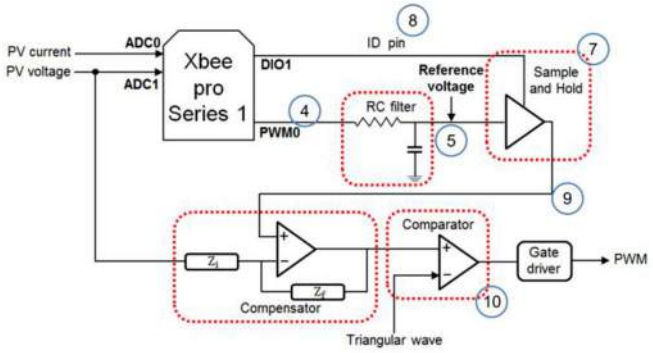

Fig. 11. Entire analog circuit configuration in the PV converter control stage.

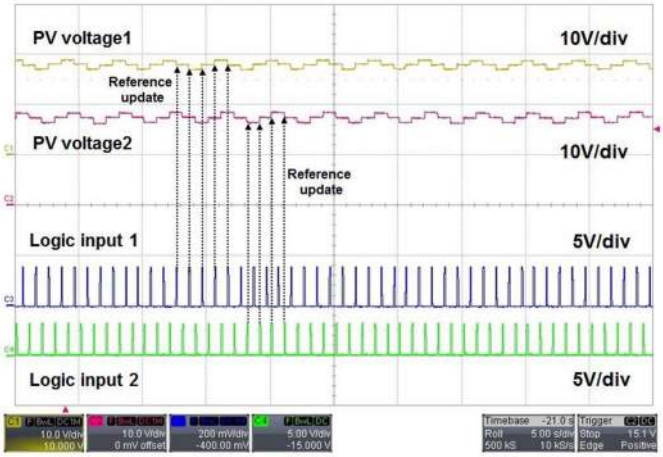

Fig. 12. Waveforms of the PV voltage and the ID pins. Logic input 1 means the ID pin 1, triggering the reference update of PV module 1.

the XBee-PRO series1, the analog data is delivered to the XBee-PRO in the PV module (no. 3) and automatically converted to PWM form (no. 4 in Fig. 11). Note that, the pin pairing method provides data transmission and conversion, i.e., from an analog input from XBee-PRO in the host to PWM output for XBee-PRO in the PV module. At the PV module, the RC filter is once again used to convert the PWM data to analog reference for the analog controller as shown in Fig. 11 (no. 5). Note that, the PWM outputs from the DSP in the host (no. 1 in Fig. 9) and for the XBee-PRO in the PV module (no. 4 in Fig. 11) become the same value.

For the RC filter, a first-order low-pass filter is applied with 100 Hz cut-off frequency and -20 dB/decade roll-off rate. The value matches the ZigBee PWM output exactly because the same TTL swing level used for the DSP is applied. Since the RC filter acquires the final analog information of the PV reference, a low-cost analog controller can be implemented, as shown in Section II.

2) Identification Operation: The unified MPPT algorithm in the host controller can create only one reference voltage at a time for the PV modules. During the analog reference transfer operation, all the PV modules receive the same reference signal simultaneously. Therefore, the PV modules must identify the signal to check if it corresponds to the module. For identification, the digital output pins for the XBee-PRO are considered the "identification (ID) pin" assigned to each PV module. From the ID pin information, the PV modules can recognize the specific PV module to which the current reference signal belongs. Therefore, the MPPT controller transmits the ID information in digital format (no. 6 in Fig. 9) along with an updated reference. The bit-stream for the ID information is also delivered to all of the PV modules simultaneously, appearing at the digital outputs (DIO0 and DIO1). However, each PV module interfaces with only one specific DIO (ID) pin. Fig. 10 shows an example of two PV modules. The local XBee-PRO constantly receives ID information as well as reference signals. Since DIO0 (ID pin 1) is connected to the next stage in PV 1 while DIO1 (ID pin 2) is connected to the same in PV 2, the analog controller can operate the corresponding reference successfully according to the ID pin signal.

The operation for the ZigBee receiver and the local analog controller is shown in Fig. 11. The reference voltage is delivered to the analog sample-and-hold device connected to the ID pin (no. 7). If the corresponding DIO pin's output is high (no. 8), the sample-and-hold device bypasses the reference value to the analog controller (no. 9). The reference value is given to the compensator as the maximum PV power voltage reference. Finally, the compensator in the controller compensates the error between the reference and real voltage by adjusting the switch-driving PWM signal (no. 10) using a triangle oscillator and a comparator.

C. Verification of the Proposed System

To validate the aforementioned recognition principle, a couple of PV module hardware prototypes with the proposed controller were implemented. The key experimental waveforms are presented in Fig. 12. It shows the PV voltage waveforms in the first and second module, and the waveforms of ID pin 1 (logic input 1) and pin 2 (logic input 2), respectively. The logic signal triggers when the reference updates in each module. Therefore, we can conclude that our proposed PV module combined with the ZigBee module follows the reference distribution between the modules. The other experimental result is presented in Section V.

IV. Simulation Results

To validate the proposed analog-controlled distributed PV module method with a single host controller, numerical

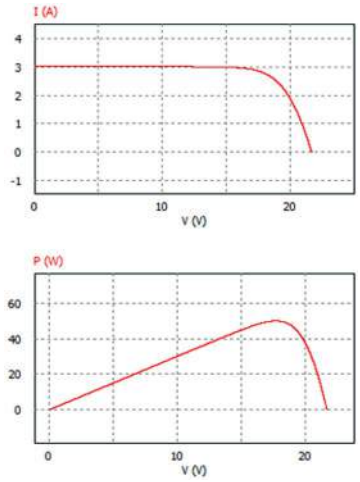

Fig. 13. PV module characteristic window.

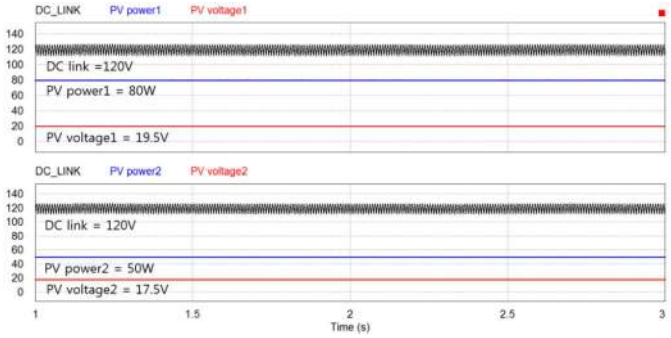

Fig. 14. Simulation result at a fixed voltage reference in each module.

analysis is performed using PSIM software. In order to apply the proposed remote control method, a couple of output-paralleled PV modules, including a boost converter, are employed. Each of the boost converters in the PV module is controlled by one of the three-pole two-zero compensators described in Section II. MPPT control is performed for PV modules 1 and 2 in turn with the help of a sample and hold part (S/H).

For the implementation of the PV panel, the PV model in PSIM is utilized. In this simulation, each module is configured with output powers of 50 and 80 W via a parameter-setting window, as shown in Fig. 13. The dc-link voltage is 120 V.

Simulation was performed for two situations. One was to evaluate the stability of the analog controller under an operating condition of varying solar radiation, and the other was to evaluate the stability of the MPPT control for different PV-characteristic curves.

Fig. 14 shows the results of the first simulation. The results confirmed that the designed compensator can stably regulate each PV module at the MPP. The low-frequency ripple from the inverter has an insignificant effect on the dc-link voltage due to the large capacitance at the link. The results of the second simulation are shown in Fig. 15 and illustrate the normal operation of the P&O MPPT method, even with different MP points for each module. For the P&O MPPT simulation, a 1 V perturbation-step and a 0.25 s step-time are applied. Fig. 16 shows one of the worst operating

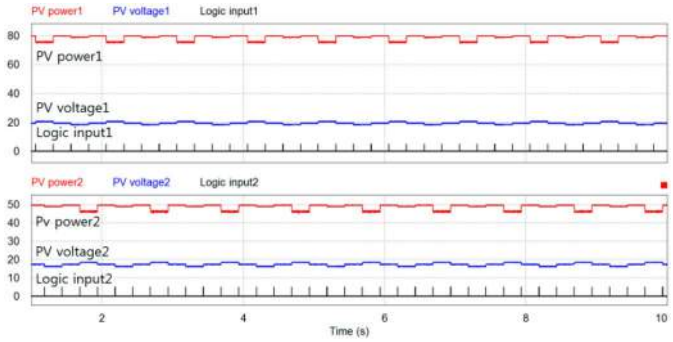

Fig. 15. Simulation result for the P&O MPPT operation under different radiation conditions.

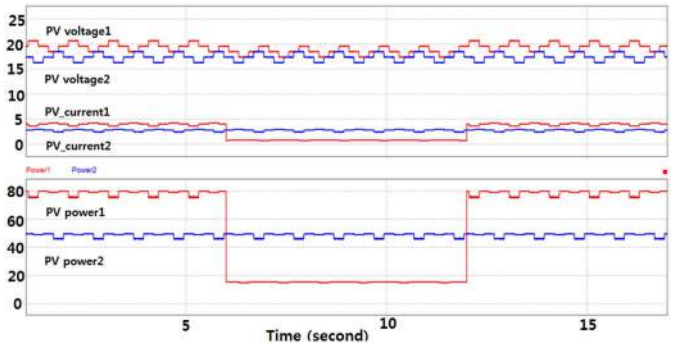

Fig. 16. Simulation result for the P&O MPPT operation under step-change irradiation conditions.

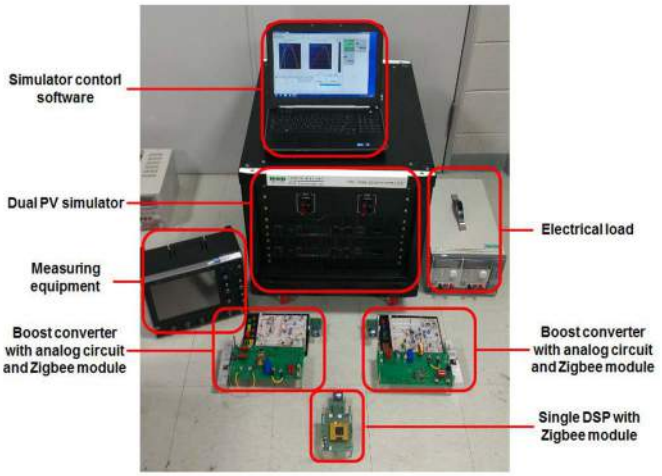

Fig. 17. Overall hardware setup.

conditions, i.e., the step-change irradiation conditions. The intensity dropped to 20% of the previous status at 6 s, but was restored at 12 s. During the shading stage, the actual MPP voltage of PV2 was 18 V and the proposed controller tracked the MPP as successfully as under the full radiation condition.

V. Experimental Verification

To validate the proposed remote MPPT control method, an experimental setup of hardware prototypes was implemented, as shown in Fig. 17. A dual PV-module simulator (TerraSAS) emulating a couple of PV panels was used along

TABLE V
KEY PARAMETERS USED IN THE EXPERIMENT

PV Panel	Dual PV-module simulator (TerraSAS)
Total DC-link	120[V]
Input Capacitor Capacitance(Vsa)	1000[uF]
Output Capacitor Capacitance	2200[uF]
Filter Inductance(L)	0.6[mH]
Switching Frequency	20[kHz]
Wireless Communication	ZigBee XBee-PRO series1
Digital signal controller	TMS320F28335

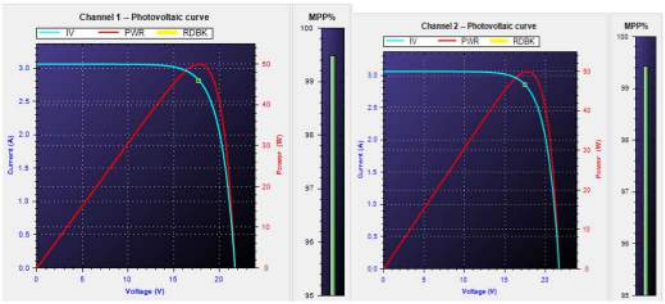

Fig. 18. 50 W *P–V* characteristic curve and MPP tracking ability.

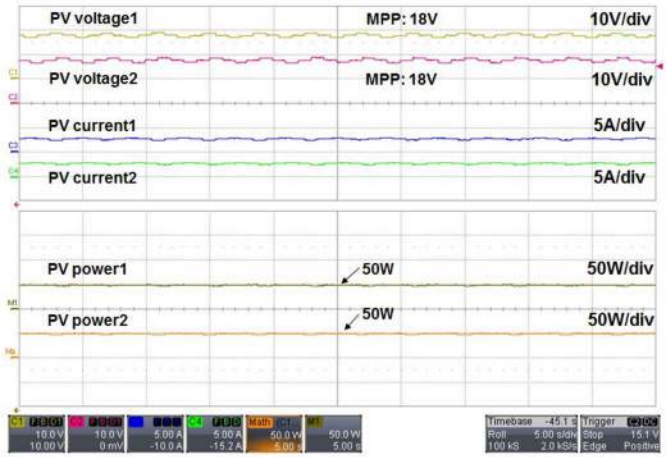

Fig. 19. Key waveforms under the same fixed MP points.

with an electronic load simulating the dc-link voltage. A communication channel was formed through ZigBee modules. The key parameters are given in Table V. For the experiment, a 50 W *P–V* curve at full radiation was applied to each module, as shown in Fig. 18. Under these operating conditions, the MPP was located at 2.8 A and 17.6 V.

The first experiment was implemented with a 50 W curve applied to each module. Under these specifications, the MPP was fixed at 17.6 V. Fig. 19 shows stable tracking operation of the PV voltage at around 18 V in both modules. The efficiency was also over 99%, as shown in Fig. 18 (vertical bar). The MPPT efficiency was obtained with the dc-link voltage fixed at 120 V and without a low-frequency fluctuation from the inverter.

In the second experiment, a whole-day profile was applied to investigate environmental variations. This profile provided variations in temperature and solar irradiance, which changed

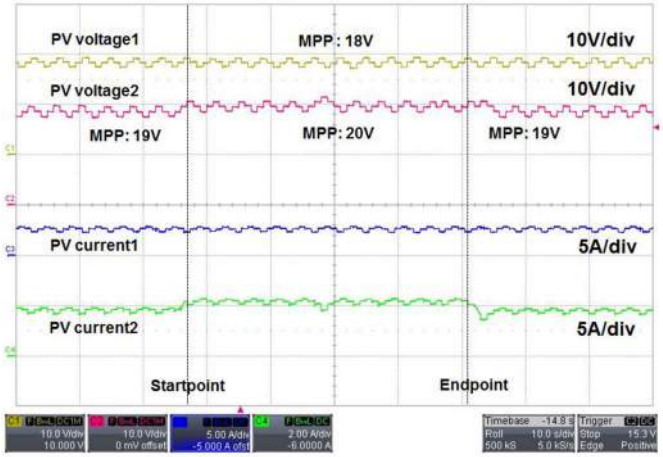

Fig. 20. Key waveforms for each module under the sunny profile.

the PV characteristic curve. In this case, the tracking ability and the dynamic speed were taken into account by accelerating the profile process time 1000-fold compared to the normal speed. In this test, the MPPT ability was evaluated according to the variation of the MP point in one of the modules, increasing from 19 to 20 V and returning to 19 V. The other module's MP point remained fixed at 18 V as shown in Fig. 18.

The experimental result is shown in Fig. 20. The range between the "start point" and "end point" reflects the time period during which the profile was applied. It can be seen that the PV voltage of module 2 increased from 19 to 20 V, then returned to 19 V, in good agreement with the real MPP profile. On the other hand, module 1 is not affected and successfully maintains the fixed MPP, since the insolation does not vary at all, as aforementioned. The three-step perturbation with a 1 V and a 1 s unit step is one of the normal operation characteristics of the P&O MPPT algorithm. The results of this experiment were in agreement with the operating principles and the simulation results.

VI. DISCUSSION

A. Cost Reduction Analysis

The experimental verification process demonstrates the actual cost savings between the MIC scheme [Fig. 1(c)] and our proposed scheme [Fig. 1(d)]. The major components for the MIC scheme are a dc–dc converter, a PV panel, a DSP, and ZigBee module for each module, a dc–ac inverter, and a central DSP and ZigBee module. On the other hand, the major components for the proposed scheme are a dc–dc converter, an analog OP-Amp, a PV panel, a ZigBee module, a dc–ac inverter, and a DSP and ZigBee module.

The cost for the MIC scheme is given as

$$\text{Cost}_{\text{MIC}}(N) = N(C_{\text{conv}} + C_{\text{PV}} + C_{\text{DSP}} + C_{\text{ZB}}) + C_{\text{inv}} + C_{\text{DSP}} + C_{\text{ZB}}$$

where N is the number of PV modules, and C_{conv}, C_{PV}, C_{ZB}, C_{inv}, and C_{DSP} denote the cost for a dc–dc MPPT tracker, one PV panel, one ZigBee module, one dc–ac inverter, and one DSP, respectively. In contrast, the cost for our

proposed scheme is

$$\text{Cost}_{\text{proposed}}(N) = N\big(C_{\text{conv}} + C_{\text{PV}} + C_{\text{OP-Amp}} + C_{\text{ZB}}\big) + C_{\text{inv}} + C_{\text{DSP}} + C_{\text{ZB}}$$

where $C_{\text{OP-Amp}}$ denotes the cost for the analog controller.

Therefore, the actual cost reduction with our proposed scheme is

$$\text{Cost}_{\text{MIC}}(N) - \text{Cost}_{\text{proposed}}(N) = N\big(C_{\text{DSP}} - C_{\text{OP-Amp}}\big).$$

Since the price for an OP-Amp is much lower than that of a DSP, it is obvious that our proposed scheme significantly reduces the overall cost of distributed PV power systems.

B. Multimodule Effects

The proposed scheme has several practical constraints for extending the number of PV modules. The maximum number of PV modules is limited by the following constraints.

The first constraint is the number of ID pins. Due to this constraint, the maximum number of the PV modules that can be managed with a single voltage reference is limited. The XBee-PRO series1 has two analog-to-PWM outputs and six channels (DIO pins). Therefore, the maximum number of PV modules is $2^6 = 64$ using the XBee-PRO series1 in the proposed scheme. Note that, Section III-B explains how the PV modules are distinguished.

The second constraint is the processing delay for the proposed scheme. Let T_{MPP} and T_d denote an MPPT update cycle and the processing delay, respectively. The processing delay is the time difference from the completion of the MPPT algorithm at the host controller (Section II-B) to the decoding of the voltage reference at each PV module. That is, it takes at least T_d seconds for the distribution of the MPPT references for a module (see Fig. 10). Therefore, the maximum number of modules is limited to $T_{\text{MPP}}/(N \cdot T_d)$ for an MPP cycle.

The third constraint comes from the bandwidth limitation of the ZigBee module. Since the proposed scheme uses 10-bit ADC resolution, 1 PV module generates only 30-bit data per T_{MPP}, which are the sampled voltage and current data as well as the voltage reference. The maximum PV module is $30 \cdot N/8 \cdot R$, where R is the maximum data rate of ZigBee.

The last constraint is the processing of the reference voltage demodulation from the PWM to the analog signal with a low-pass filter (see RC filters in Figs. 9 and 11). Because the filter presents a phase-delay, too many modules can make it hard to allocate each of the reference signals to the corresponding module at the exact sampling time (see Fig. 10). The effect can be estimated exactly in the same manner as the propagation delay mentioned above.

Fig. 21 presents the circuit diagrams of four PV-module systems with a propagation delay for checking MPPT by PSIM simulation. The MPPT operating points of the four modules are 29, 24, 20, and 15 V. Fig. 22 shows the key waveforms for each module and the results confirm that the multimodal system worked well with the MPPT controller despite the partial-shading conditions, the ZigBee propagation delay, and the demodulation low-pass filter.

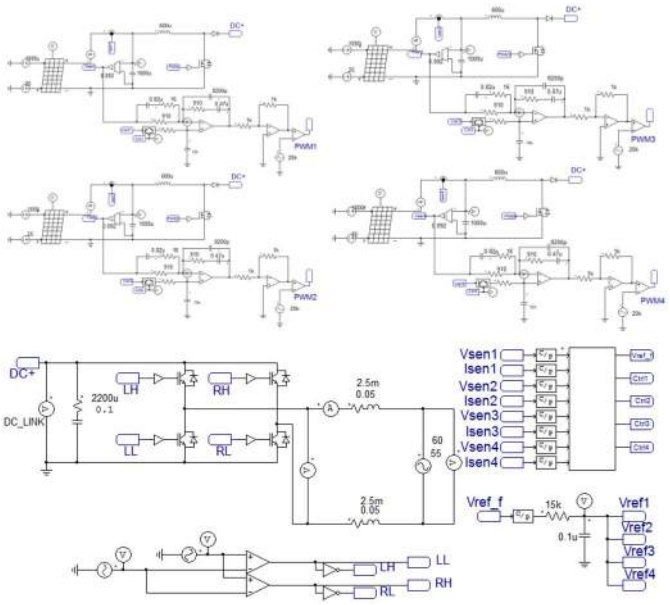

Fig. 21. Circuit diagrams of four PV-module systems with a propagation delay for checking the MPPT by PSIM simulation.

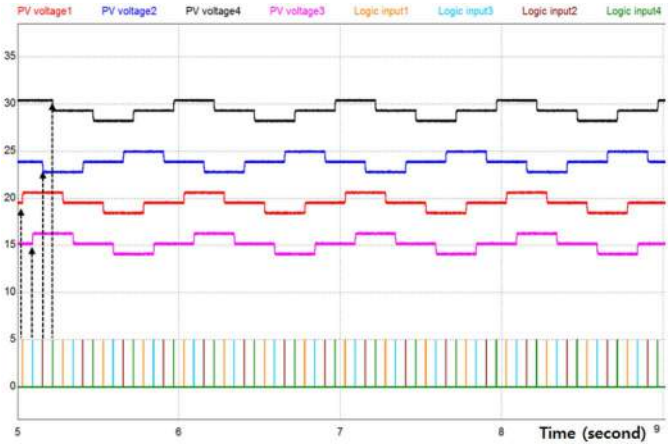

Fig. 22. Key waveforms of the each module on different MP point.

Note that, our proposed control architecture can also be applied to a microgrid power system. However, ZigBee might not be enough to exchange the sensing data and control messages within the microgrid according to practical constraints. This is because the microgrid covers much broader ranges and more PV modules than the in-building system. Therefore, another communication system is needed to satisfy these requirements, such as Wi-Fi or WiMAX [26].

VII. Conclusion

In this paper, a new control architecture was proposed to reduce the cost of multiple PV PCSs. It consists of a single MPPT controller system at the host and simple analog controllers in remote PV modules, with ZigBee modules connecting the host and remote PV modules. Conventionally, one MPPT control circuit is used to track the local maximum power point for each PV module, resulting in high-material cost. Using ZigBee wireless networks, the proposed system

substituted an analog circuit for the distributed digital MPPT control circuit at the PV module, which is the key to cost reduction. The proposed algorithm was verified experimentally for an output-paralleled boost-type multimodal PCS. The MPPT performance for the hardware prototype of the PV module was over 99%, and the feedback controller demonstrated stable operation. Under the full radiation and unbalanced variable condition of dual PV simulators, MPPT tracking capability tests verified stable and accurate operation of the proposed algorithm even under the transient condition.

REFERENCES

[1] R. Eke and A. Senturk, "Monitoring the performance of single and triple junction amorphous silicon modules in two building integrated photovoltaic (BIPV) installations," *Appl. Energy*, vol. 109, pp. 154–162, Apr. 2013.

[2] B. Celik, E. Karatepe, N. Gokmen, and S. Silvestre, "A virtual reality study of surrounding obstacles on BIPV systems for estimation of long-term performance of partially shaded PV arrays," *Renew. Energy*, vol. 60, pp. 402–414, Dec. 2013.

[3] M. D'Orazio, C. Perna, and E. Giuseppe, "Experimental operating cell temperature assessment of BIPV with different installation configurations on roofs under Mediterranean climate," *Renew. Energy*, vol. 68, pp. 378–396, Mar. 2014.

[4] W. Cai, B. Liu, S. Duan, and L. Jiang, "An active low-frequency ripple control method based on the virtual capacitor concept for BIPV systems," *IEEE Trans. Power Electron.*, vol. 29, no. 4, pp. 1733–1745, Apr. 2014.

[5] J.-M. Choe, B.-J. Byen, and G.-H. Choe, "Parallel PCS interconnection current surge elimination technique using a coupled inductor," *J. Power Electron.*, vol. 14, no. 5, pp. 827–833, Sep. 2014.

[6] Z. Ozkan and A. M. Hava, "Classification of grid connected transformerless PV inverters with a focus on the leakage current characteristics and extension of topology families," *J. Power Electron.*, vol. 15, no. 1, pp. 256–267, Jan. 2015.

[7] S. Yousofi-Darmian and S. M. Barakati, "Transformer-less single-phase four-level inverter for PV system applications," *J. Power Electron.*, vol. 14, no. 6, pp. 1233–1242, Nov. 2014.

[8] S.-J. Park, J.-H. Shin, J.-H. Park, and H.-J. Jeon, "Dynamic analysis and controller design for standalone operation of photovoltaic power conditioners with energy storage," *J. Elect. Eng. Technol.*, vol. 9, no. 6, pp. 2004–2012, Nov. 2014.

[9] S.-T. Kim, T.-H. Bang, S.-C. Lee, and J.-W. Park, "Real-time maximum power point tracking method based on three points approximation by digital controller for PV system," *J. Elect. Eng. Technol.*, vol. 9, no. 5, pp. 1447–1453, Sep. 2014.

[10] D.-H. Kim, G.-Y. Cheo, and B.-K. Lee, "Design and control of an optimized battery charger for an xEV based on photovoltaic power systems," *J. Elect. Eng. Technol.*, vol. 9, no. 5, pp. 1602–1613, Sep. 2014.

[11] J. H. Park, J. Y. Ahn, B. H. Cho, and G. J. Yu, "Dual-module-based maximum power tracking control of photovoltaic systems industrial electronics," *IEEE Trans. Ind. Electron.*, vol. 53, no. 4, pp. 1036–1047, Aug. 2006.

[12] R. W. Erickson and A. P. Rogers, "A microinverter for building-integrated photovoltaics," in *Proc. Appl. Power Electron. Conf. Expo.*, Washington, DC, USA, 2009, pp. 911–917.

[13] N. Femia, G. Lisi, G. Petrone, G. Spagnuolo, and M. Vitelli, "Distributed maximum power point tracking of photovoltaic arrays: Novel approach and system analysis," *IEEE Trans. Ind. Electron.*, vol. 55, no. 7, pp. 2610–2621, Jul. 2008.

[14] R. Kadri, J.-P. Gaubert, and G. Champenois, "Non-dissipative string current diverter for solving the cascaded DC–DC converter connection problem in photovoltaic power generation system," *IEEE Trans. Power Electron.*, vol. 27, no. 3, pp. 1249–1258, Mar. 2012.

[15] A.-Y. Jung, J.-H. Park, and H.-J. Jeon, "Analysis and design of phase-interleaving series-connected module-integrated converter for DC-link ripple reduction of multi-stage photovoltaic power systems," *Progr. Photovolt. Res. Appl.*, vol. 21, no. 5, pp. 1189–1203, Aug. 2013.

[16] S. Moon, D.-H. Kim, C.-I. Kim, D. T. Thayalan, and J.-H. Park, "Single MPPT controller for multi-module converters using wireless communication," in *Proc. 7th Int. Power Electron. Motion Control Conf. (IPEMC)*, Harbin, China, Jun. 2012, pp. 1368–1371.

[17] X. Xiaoli and Q. Daoe, "Remote monitoring and control of photovoltaic system using wireless sensor network," in *Proc. Int. Conf. Elect. Inf. Control Eng. (ICEICE)*, Wuhan, China, 2011, pp. 633–638.

[18] M. Vitelli, "On the necessity of joint adoption of both distributed maximum power point tracking and central maximum power point tracking in PV systems," *Progr. Photovolt. Res. Appl.*, vol. 22, no. 3, pp. 283–299, Mar. 2014.

[19] M. Balato and M. Vitelli, "A new strategy for the identification of optimal operating points in PV applications with distributed MPPT," in *Proc. Int. Conf. Exhibit. Ecol. Veh. Renew. Energies (EVER)*, Monte Carlo, Monaco, Mar. 2013, pp. 1–6.

[20] M. Balato and M. Vitelli, "A hybrid MPPT technique based on the fast estimate of the maximum power voltages in PV applications," in *Proc. Int. Conf. Exhibit. Ecol. Veh. Renew. Energies (EVER)*, Monte Carlo, Monaco, Mar. 2013, pp. 1–7.

[21] S.-J. Kim, S. Moon, D.-H. Kim, J.-H. Park, and C.-S. Chung, "Photovoltaic maximum power point tracking without current sensor for module integrated converter," in *Proc. Int. Conf. Elect. Mach. Syst. (ICEMS)*, Beijing, China, Aug. 2011, pp. 1–5.

[22] S. Moon *et al.*, "Maximum power point tracking without current sensor for photovoltaic module integrated converter using ZigBee wireless network," *Int. J. Elect. Power Energy Syst.*, vol. 56, pp. 286–297, Mar. 2014.

[23] J.-S. Lee, Y.-W. Su, and C.-C. Shen, "A comparative study of wireless protocols: Bluetooth, UWB, ZigBee, and Wi-Fi," in *Proc. IEEE Ind. Electron. Soc.*, Taipei, Taiwan, Nov. 2007, pp. 46–51.

[24] Z. Fadlullah *et al.*, "Toward intelligent machine-to-machine communications in smart grid," *IEEE Commun. Mag.*, vol. 49, no. 4, pp. 60–65, Apr. 2011.

[25] Digi International Inc. (Jun. 10, 2014). *XBee/XBee-PRO RF Modules*. [Online]. Available: http://www.digi.com/support/

[26] P. Parikh, M. Kanabar, and T. Sidhu, "Opportunities and challenges of wireless communication technologies for smart grid applications," in *Proc. IEEE Power Energy Soc. Gen. Meeting*, Minneapolis, MN, USA, Jul. 2010, pp. 1–7.

Sol Moon received the B.S. and M.S. degrees from the Department of Electrical Engineering, Soongsil University, Seoul, Korea, in 2011 and 2013, respectively.

His current research interests include the analysis and design of high-frequency switching converters, electric vehicles, and renewable energy applications.

Sung-Guk Yoon (M'13) received the B.S. and Ph.D. degrees from the Department of Electrical and Computer Engineering, Seoul National University, Seoul, Korea, in 2006 and 2012, respectively.

From 2012 to 2014, he was a Postdoctoral Researcher with Seoul National University. He has been an Assistant Professor with Soongsil University, Seoul, since 2014. His current research interests include microgrid and power line communications.

Joung-Hu Park (S'02–M'06–SM'13) received the B.S., M.S., and Ph.D. degrees from the Department of Electrical Engineering and Computer Science, Seoul National University, Seoul, Korea, in 1999, 2001, and 2006, respectively.

He is currently an Assistant Professor with Soongsil University, Seoul. His current research interests include the analysis of high-frequency switching converters and renewable energy applications.